INNOVATIVE AIRSHIP DESIGN FOR REAL-TIME AIR QUALITY MONITORING USING IOT TECHNOLOGY

Sudhir Jain Prathik[1], Athimoolam Sundaramahalingam[1], Sudhagara Rajan S[2], Jenoris Muthiya Solomon[3], Chethan K. N[4]*, Laxmikant G Keni[4]*

[1] Department of Aeronautical Engineering, Dayananda Sagar College of Engineering, Karnataka, India
[2] Department of Aerospace Engineering, School of Mechanical Engineering, REVA University, Karnataka, India
[3] Department of Automobile Engineering, Dayananda Sagar College of Engineering, Karnataka, India
[4] Department of Aeronautical & Automobile Engineering, Manipal Institute of Technology, Manipal Academy of Higher Education, Karnataka, India.
chethan.kn@manipal.edu; laxmikant.keni@manipal.edu

The effect of poor air quality on human health has been linked to both short-term and long-term exposure to air pollutants. One of the most important steps in reducing emissions is accurate identification of these pollutants. This can be achieved by using Internet of Things equipped remotely operated airships that can survey large areas and gather pollution data. The ability of an airship to function at low altitudes for extended periods is the main design requirement of airships. This study describes a methodology for conceptualizing and building a helium-filled blimp for remote measurement of atmospheric pollutants (Carbon monoxide, Carbon dioxide, and Sulphur dioxide), temperature, and pressure. An onboard telemetry system measures the data while the airship is in flight and transmits them in real time to a ground-based station. The experiment showed that remotely operated airships are capable of gathering air data and their quality, enabling environmental scientists and regulatory agencies to better understand the behaviour of air pollutants and take steps to mitigate them.

Keywords: airships, helium, air quality, internet of things

1 INTRODUCTION

The amount of carbon emissions has steadily increased since the 19th century. The major reason for this rise in dangerous pollutants, such as carbon monoxide (CO), sulfur oxides (SOx), and nitrogen oxides (NOx) is the increased use of machinery instead of human efforts. The primary human activities causing the release of these pollutants are the increased use of fossil fuels and vehicles. Since we are moving towards the objective of achieving zero carbon emissions by 2050, reduction and continuous monitoring of these pollutants is essential. Increased air pollution levels can have several detrimental effects on health, such as lung cancer, heart disease, allergies, and respiratory problems. Currently, satellites, ground stations, and laboratory sampling are the main methods used to monitor air pollution. Ground stations have a limited range that typically covers only a small radius. However, ground sampling offers greater accuracy and is time-consuming. Satellites have significantly expanded the range and accuracy of monitoring but are limited by their inability to operate effectively under rainy or cloudy conditions [1].

To bridge the gap between the advantages of ground-based stations and satellites, an airship equipped with Internet of Things (IoT) technology is introduced in this work which is capable of measuring pollutants and updating to the ground station server in real-time. An airship is a powered and controllable aircraft. To achieve lift, it relies on its buoyancy, obtained from a lifting gas with a lower density than the surrounding air. Hydrogen provides the highest lifting capacity per unit volume; however, it is highly flammable. However, helium, which is non-flammable, has a slightly lower lifting capacity and is more expensive. The outer envelope of an airship can be made from a single gas bag or a separate supported skin. An airship comprises an envelope, as well as engines, crew, and payload support, which are normally housed in a gondola suspended below the envelope. Airships can be divided into three categories according to their structural arrangement: semi-rigid, rigid, and non-rigid. Non-rigid airships rely solely on the pressurized envelope for support, whereas rigid airships have a heavily rigid structure placed internally. Semi-rigid airships contain a supporting structure known as a keel, which runs along the length of the airship and supports a flexible envelope. In addition, the keel serves as a place to attach fans and motors, spreading the weight uniformly throughout the airship.
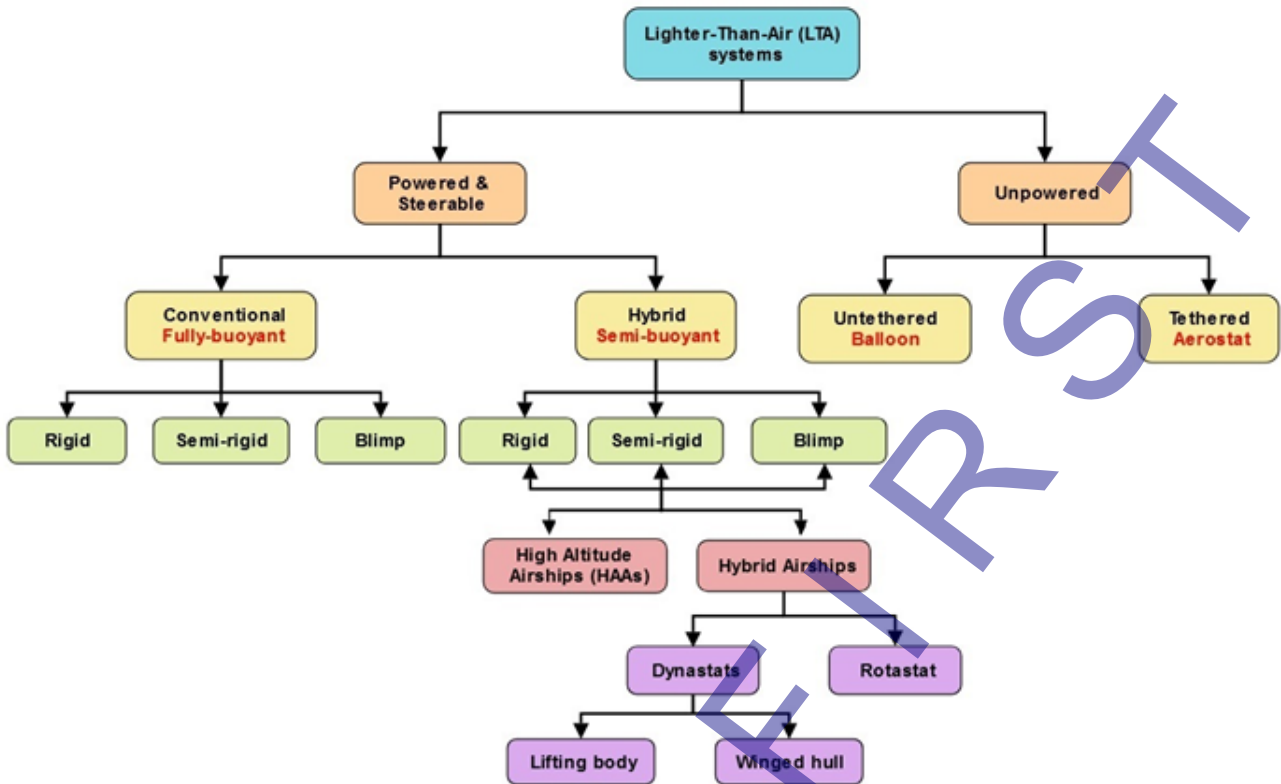
Fig. 1. Classification of LTA systems

The gondola, engines, and empennage are attached to the hull framework and/or keel, with the framework responsible for evenly distributing the loads throughout the hull surface. Non-rigid airships are commonly used for remote-control applications owing to their ease of fabrication, transportability, and low weight. However, in this configuration, the engines and payload are typically installed only on the gondola, which is mounted below the envelope [2]. Figure 1 shows the complete classification of Lighter-Than-Air (LTA) systems.

The use of an airship offers distinct advantages over other unmanned aerial vehicles (UAVs) because it generates lift through the buoyancy of helium, requiring minimal effort to carry the payload. While UAVs excel in agility, real-time response, and specialized tasks, airships supplement these qualities with endurance, cargo capacity, stability, and operational efficiency. As a result, the need for airships exists in a variety of industries where their distinct capabilities give significant value over the UAVs that are offering in the present scenario. IoT devices comprise computer devices, actuators, software, and wireless sensors. They are affixed to a device that functions over the Internet, permitting an automatic, human-free exchange of data between things or individuals. The airship in this work is equipped with sensors, such as carbon monoxide optical dust sensors and SO_x sensors, which work in conjunction with the IoT device to measure pollutant levels in the air.

2 MATERIAL AND METHODS

In relation to airship design, Figure 2 provides a concise overview of the design methodology that needs to be adhered to. The process involves multiple iterations until the lift-total weight value exceeds the payload requirement, thereby ensuring that the airship remains statically heavier. Engineering design comprises three distinct phases: conceptual, preliminary, and detailed. The conceptual design phase takes about 5% of the total to complete, is the shortest of these stages in terms of time and requires the least investment. Nevertheless, the decisions taken in this phase have a direct impact on the effort and investment of the subsequent phases; therefore, its importance should not be undervalued. Design studies are vital components of the conceptual design phase because they help determine the basic requirements of the project.

These studies involve a sensitive analysis to ascertain the effect of design variables on the performance and operational parameters. This methodology also allows designers to investigate the consequences of adding particular design features or choosing from a variety of design possibilities, as well as to carry out sensitivity studies concerning design parameters.
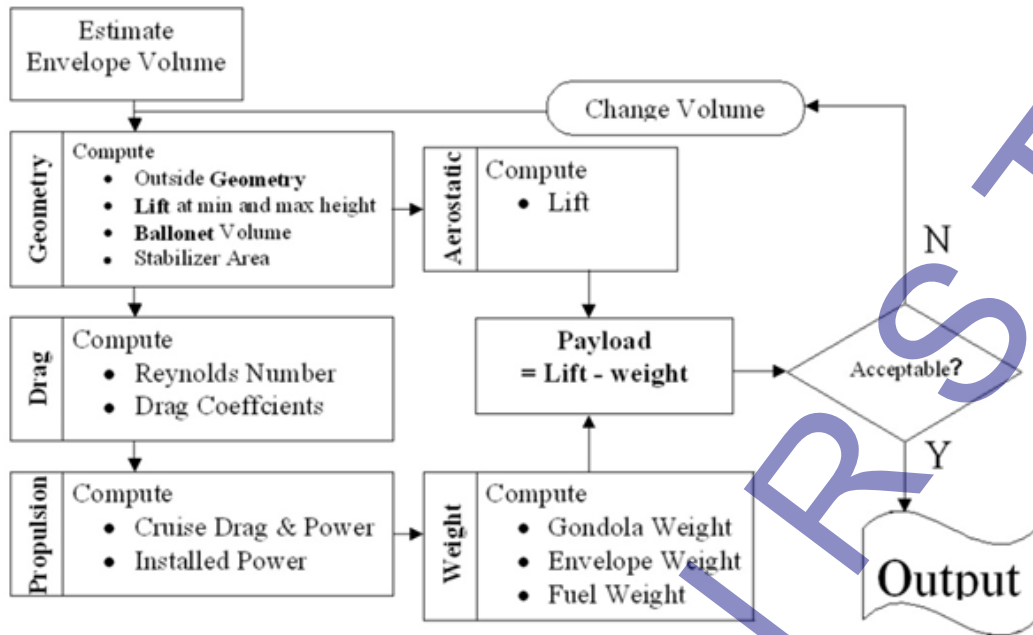
Fig. 2. Flowchart for sizing of airship

2.1 Selection of envelope shape

The envelope is a vital component of airships and is significant. While selecting the shape of the envelope, aerodynamic aspects are primarily considered in addition to structural and manufacturability aspects. Although ellipsoidal shapes are the most common for aerostats and airships, other non-conventional shapes and configurations have also been used, with the advantages and disadvantages associated with each [3]. These include spherical [4], winged airship [5], dart, deltoid, flat body [6], lenticular [7], toroidal [8], torus [9], multi balloon [10], and multihull [11], [12]. To improve aerodynamic performance, modifications to the conventional ellipsoidal shape have also been investigated, such as the addition of parabolic and circular arc components. Non-conventional airship envelope shapes, although providing distinct advantages in particular circumstances, also have a number of drawbacks, including design complexity, manufacturing challenges, operating limits, being less ideal across a wide variety of flying conditions, etc.

In IIT Bombay, a micro-airship was developed and tested in flight to provide a preliminary evaluation of the geometrical nonrational volume (GNVR) shape suitability for the airship envelope. This micro-airship had favorable drag characteristics, with a maximum speed of approximately 25 km/h. Due to number of benefits, small airships or blimps frequently employ the GNVR shape, usually referred as "blimp shape" as shown in Figure 3.

Nose Ellipse - origin to 1.25d: $\frac{x^2}{1.25d^2} + \frac{y^2}{0.5d^2} = 1$

Middle Circle - 1.25d to 1.62d: $x^2 + (y - 3.5d)^2 = 16d^2$

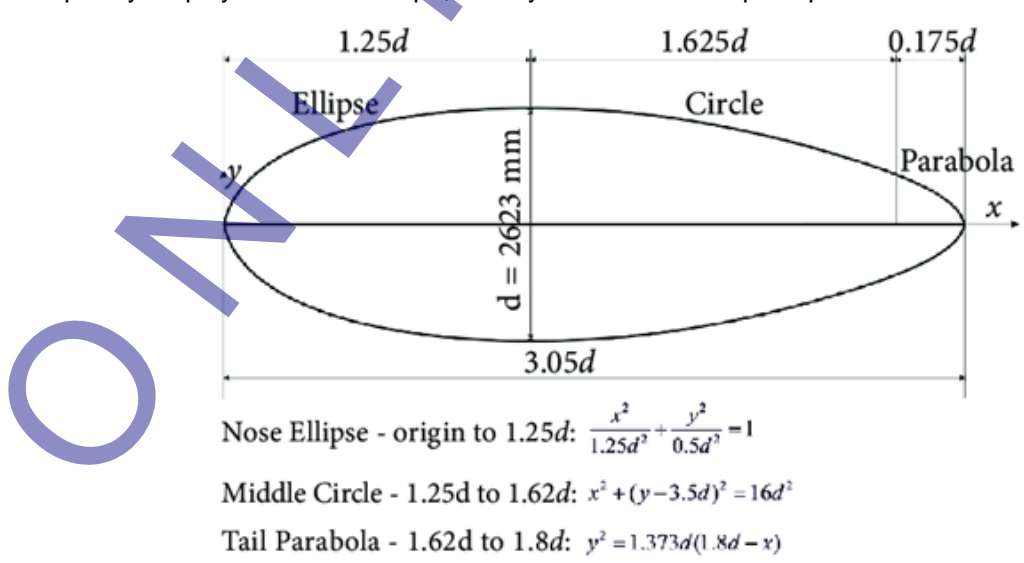Tail Parabola - 1.62d to 1.8d: $y^2 = 1.373d(1.8d - x)$

Fig. 3. Nomenclature of GNVR shape

The GNVR shape has the virtue of being both stable and easy to control. The distribution of the envelope volume around the center of mass minimizes the impact of external forces such as wind gusts, which makes it easier to maintain a stable hover and maneuver the airship with precision. The GNVR shape also makes manufacturing

simpler and more cost effective. By constructing an envelope from a single piece of material, the airship's aerodynamic efficiency is increased, and the number of seams is reduced. Overall, the GNVR shape is a better option for small airships because it offers stability, control, and economies of scale, which makes it an ideal choice for a range of applications, such as research, advertising, and surveillance.

2.2 Lift estimation

To determine the lift force generated by the lifting gas, equations accounting for various parameters must be developed. The assumptions considered while arriving at the fundamental equation for buoyant force are that the surrounding air is dry, the lifting gas is pure, and the lifting gas completely fills its container. From the Navier-Stokes equation 1, the buoyant force was calculated as follows:

$$Buoyant\ Lift(L) = Volume * g * (\rho_{air} - \rho_{He}) \tag{1}$$

Where, L is the Buoyant lift, g is the acceleration due to gravity and ρ_{air} & ρ_{He} are the density of air and helium respectively.

However, this equation assumes that air and lifting gases share the same temperature and that the pressure remains constant. If both air and lifting gas experience an equal change in temperature, the buoyant lift remains unchanged. Therefore, the net lift (L_n) and gross lift (L_g) can be expressed as:

$$L_n = \text{Volume} * g * (\rho_{air} - \rho_{He}) \tag{2}$$

$$L_g = \text{Volume} * g * \rho_{He} \tag{3}$$

2.3 Drag estimation

Because the drag coefficient affects the amount of power required by an air-ship to carry out its mission, accurately estimating the drag coefficient of an air-ship is essential. The envelope's drag constitutes the majority of an airship's total drag because it is a low-speed bluff body. Therefore, most airship envelopes are axisymmetric about the line of flight or bodies of revolution to lessen total drag. First, the assumptions are made via turbulent flow over the hull, and the drag was estimated in terms of the drag coefficient (C_{dv}), max velocity (V_{cr}), volume (V), and reference area (S) is given in equation 4:

$$D = \frac{1}{2} * C_{dv} * \rho_{air} * (V_{cr})^2 * S \tag{4}$$

The drag coefficient (C_{dv}), viscosity (μ), and Reynolds number for the flow were cal-culated using the expression given below. Viscosity (μ) was calculated using:

$$\mu = 1.7140 * 10^{-5} * \left(\frac{(T_s + \Delta T)}{273}\right)^{4.256} \tag{5}$$

where Ts is the standard atmospheric temperature and ΔT is the temperature above the standard atmospheric temperature.

Reynolds number was estimated using:

$$Re = \frac{\rho_{air} * v * l}{\mu} \tag{6}$$

As per Hoerner [13], the drag coefficient over the envelope is given by:

$$\frac{C_{dv}}{C_f} = 4(f)^{\frac{1}{3}} + 6\left(\frac{1}{f}\right)^{\frac{7}{6}} + 24\left(\frac{1}{f}\right)^{\frac{8}{3}} \tag{7}$$

$$C_f = \frac{0.045}{Re^{\frac{1}{6}}} \tag{8}$$

$$C_{dv} = \frac{0.18 * (f)^{1/3} + 0.27 * (f)^{-7/8} + 1.08 * (f)^{-8/3}}{Re^{\frac{1}{6}}} \tag{9}$$

where, f = l/d = fineness ratio, Re = Reynolds number based on the length of the envelope, C_f = skin friction coefficient, l = length of the envelope, d = maximum diameter of the envelope, and ρ_{air} = air density.

2.4 Payload selection

The payload in our aspect are the sensors, IoT, and miscellaneous items that are needed to complete the circuit.

2.4.1 IOT selection

Currently, the market has two prominent IoT devices, Raspberry Pi and Arduino. After conducting extensive research, it was discovered that Arduino is compatible with all gas sensors and SIM modules, a feature lacking in Raspberry

Pi. Furthermore, Arduino (Figure 4 (a)) is generally regarded as more user-friendly and easier to program than the Raspberry Pi. It employs a simpler and more intuitive programming language specifically designed for straightforward electronic projects. In contrast, the Raspberry Pi is better suited for complex endeavors that demand increased processing capabilities. Additionally, Arduino boards are generally more affordable than Raspberry Pi boards, making them preferable for uncomplicated projects that do not require significant processing power or extensive connectivity options.

2.4.2 Sensor selection

The MQ7 and MQ135 sensors shown in Figure 4 (b) and 4 (c) were used to measure the amount of pollutants present in the surrounding air. They are made of tin oxide (SnO_2), which has lower conductivity in pure air. As the concentration of the CO gas increased, the conductivity of the sensor also increased. MQ7 was used to detect the amount of CO in the atmosphere. The MQ-135 sensor has a high sensitivity to ammonia, sulfide, and benzene-based vapors and is ideal for monitoring smoke and other harmful gases. The Gallium Arsenide Phosphide Infrared Emitting Diode (GaAsP) and Silicon NPN Phototransistor (GP2Y Series), shown in Figure 4 (d), are infrared (IR) proximity sensors. It shines a beam of IR light from an LED and measures the intensity of the light that is bounced using a phototransistor. This IR sensor offers significantly better performance than existing IR alternatives and is more affordable than sonar-range finders. A microelectromechanical system pressure sensor (MPL3115A2) produced by NXP Semiconductors is depicted in Figure 4(e). It is a compact, low-power sensor that is ideal for a range of applications, including weather stations, altimeters, and drones, because it offers precise readings of pressure and altitude.
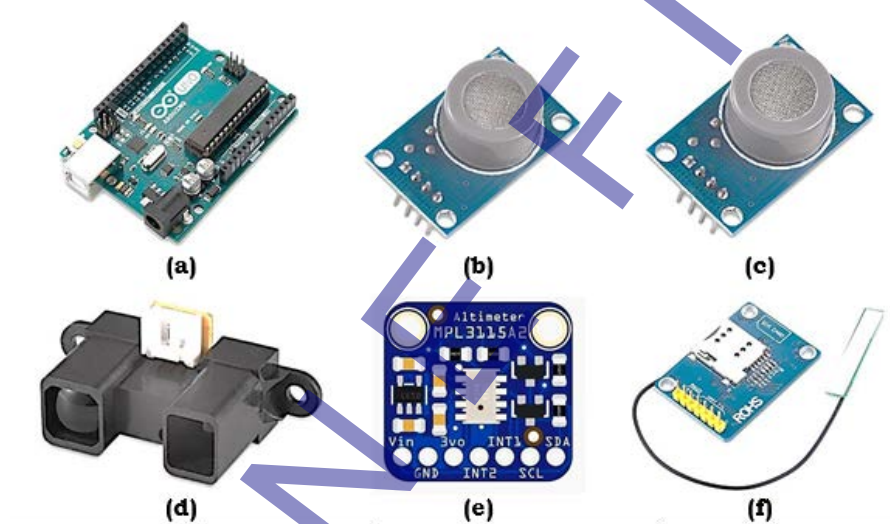

Fig. 4. IoT and Sensors used (a) Arduino Uno - R3, (b) MQ-7 Sensor, (c) MQ-135 Sensor, (d) GP2Y Sensor, (e) MPL3115A2 Sensor and (f) SIM800L Sim module

SIM800L (Figure 4 (f)) is a type of small and low-power GSM/GPRS (Global positioning system/General Packet Radio Service) module manufactured by SIM Com Wireless Solutions. It is designed to provide wireless communication capabilities to electronic devices and systems such as remote monitoring systems, (GPS) trackers, and other IoT applications. The SIM800L module supports various communication standards, including GSM, GPRS, and short message service (SMS), and can be controlled using Attention (AT) commands over a serial interface. This module is known for its compact size, low power consumption, and reliable performance, making it ideal for battery-powered and portable devices. The weight breakdown of the payloads used in this study is presented in Table 1.

Table 1. Payload weight breakdown

Payload	Weight (grams)
Arduino	25
MQ7- Sensor	10
MQ135 - Sensor	12
MPL3115A2 – Pressure sensor	8
GP2Y0A02YK0F, GPS Sensor	40
Wires	40
Breadboard	97
Total	232

2.5 Material selection

Given that the dimensions of the airship were fixed, the materials needed to build the entire airship were selected based on a few constraints.

2.5.1 Envelope material

An envelope material Polyvinyl chloride (PVC) sheet was chosen because of its good helium retention properties and excellent breaking strength. A stress test was performed to determine the maximum stress experienced by the material during the lifetime operation of the airship. The pressure exerted by the gas was measured using equations (10-13) and compared with the safety factor of the material to determine if it was significantly below the limit. The following three primary types of pressure are considered:

ΔP_{int} = Internal pressure, ΔP_{head} = Hydrostatic loading, ΔP_a= Aerodynamic Loading

$$\text{Stagnation pressure}, P_0 = 1/2 * \rho_{air} * v^2 = 9.8048 \ \frac{N}{m^2} \tag{10}$$

Assuming that the differential pressure at the centerline was 1.15 times the maximum dynamic pressure and C_p = 0.3 to 0.35, [14]

$$\Delta P_{int} = 1.15 * 9.8048 \ = \ 11.2755 \ \frac{N}{m^2} \tag{11}$$

$$\Delta P_a = \frac{1}{2} * \rho_{air} * v^2 * C_p = 3.2355 \ \frac{N}{m^2} \tag{12}$$

$$\Delta P_{head} = (\rho_{air} - \rho_{He})g * \frac{d}{2} \tag{13}$$

From Figure 3, for L= 4.5 m, d = 1.1474 m and ρ_{air} = 1.2256 kg/m³ and ρ_{He} = 0.169 kg/m³. Hence, ΔP_{int}, ΔP_{head}, ΔP_a and ΔP_{total} were found to be 11.2755 N/m², 5.947 N/m², 3.2355 N/m² and 21 N/m². The circumferential unit load was found to be $(\Delta P * R)$=12.408 N/m². Since the maximum load carrying capacity of PVC 4.76 kg/cm² [15] is far higher than the total load, it is safe to proceed with the selected material.

2.5.2 Gondola and tail fin selection

The construction materials for Gondola were evaluated according to their strength, weight, and ease of fabrication. Table 2 lists the characteristics of various materials. After analyzing the costs, densities, and strengths of the various materials, it is best to proceed with defron reinforced with balsa to strengthen the material. Although acrylic sheets are a more favorable choice, creating cuts and holes is a challenging task. It is also p referable to reduce the weight because the gondola will only be housed in IoT devices, batteries, and cockpit electronics. Depron was chosen for the tail fin because it is strong and lightweight, although it is a wise precaution to reinforce it with balsa wood.

Table 2. Properties of Various Materials [16]

Parameters	Depron	Light density polyethylene	Acrylic sheet	Aluminium	Bamboo	Balsa wood
Density (kg/m3)	350	950	1190	2700	350	150
Strength (MPa)	500	25	65	100-350	16	19.9

2.5.3 Avionics selection

Taking the thrust requirement (equal to drag) from equation (4), two 2200 kV brushless DC motors (Figure 5 (a)) along with 6" x4" APC propellers (Figure 5 (b)) were chosen, each capable of delivering a thrust of 200 g. To regulate the speed, 30 Amp electronic speed controllers (Figure 5 (c)) were employed. Figure 5 (d) illustrates a 5000 mAh Lithium polymer (Li-Po) two-cell battery with a maximum discharge rate of 50C. The transmitter sends commands to the receiver through a set radio-frequency signal. In this work, the RCB6i 6-channel 2.4 GHz transmitter and avionic RZ6 6-channel receiver are used; they are depicted in Figures 5(e) and (f), respectively.
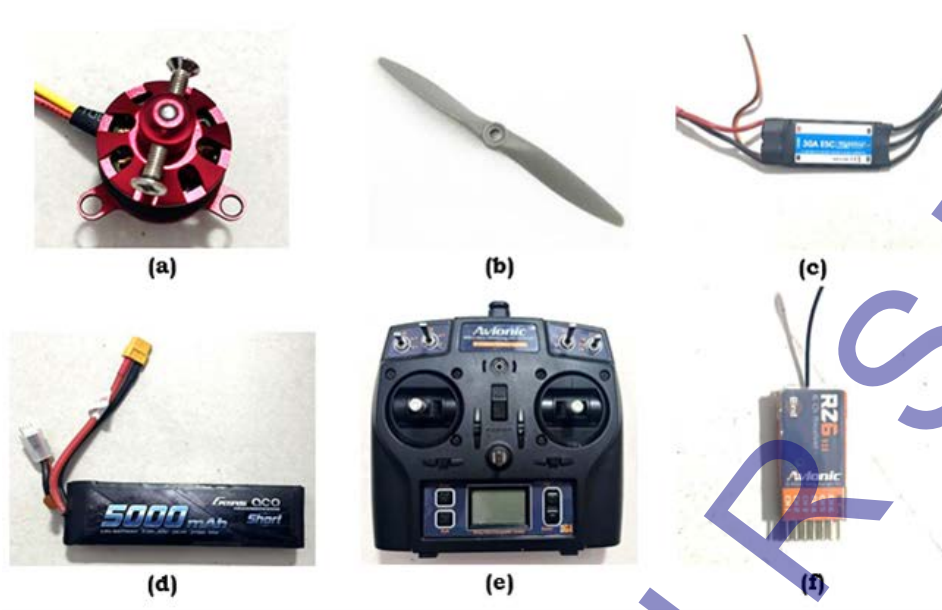
Fig. 5. Avionics (a) BLDC motor, (b) Propeller, (c) Electronic speed controller, (d) Lithium polymer battery, (e) Transmitter and (f) Receiver

2.5.4 Weight breakdown

All required materials were purchased, and each was weighed on a weighing scale. Table 3 lists the weight of each component.

Table 3. Complete Weight Breakdown of the Airship.

Item	Weight (g)
Envelope	4114
Motor*2	30
Gondola	120
Receiver	20
Battery Pack	265
Propellers	30
Wires	25
Breadboard	95
Fin Weight	350
Payload	235
Total Weight	5284

The net lift obtained from Equation (2) is 5006.42 grams which is less than the total weight (5284 g). This condition ensures that the airship is statically heavy so that it always decreases slowly when thrust is not given, which acts as a safety measure for the system.

3 RESULTS AND DISCUSSIONS

3.1 Petal Design

The coordinates of the GNVR shape were scaled down to match the micro-airship length. A fourth-order polynomial fit [17] given in Equation (14) is generated using these coordinates, and the cross-sectional shape of the envelope is generated. The envelope was manufactured in four petals for ease and accuracy in fabrication, as well as to minimize wastage of the fabric. The coordinates of the petals were generated along their length. Figure 6 shows a sketch of the gore petal made of a single panel.

$$y = -3\text{E} - 12x^4 + 4\text{E} - 08x^3 - 0.0003x^2 + 0.6943x^1 - 21.34 \qquad (14)$$

$$R^2 = 0.9992$$

Sudhir Jain Prathik et al. - Innovative airship design for real-time air quality monitoring using IoT technology
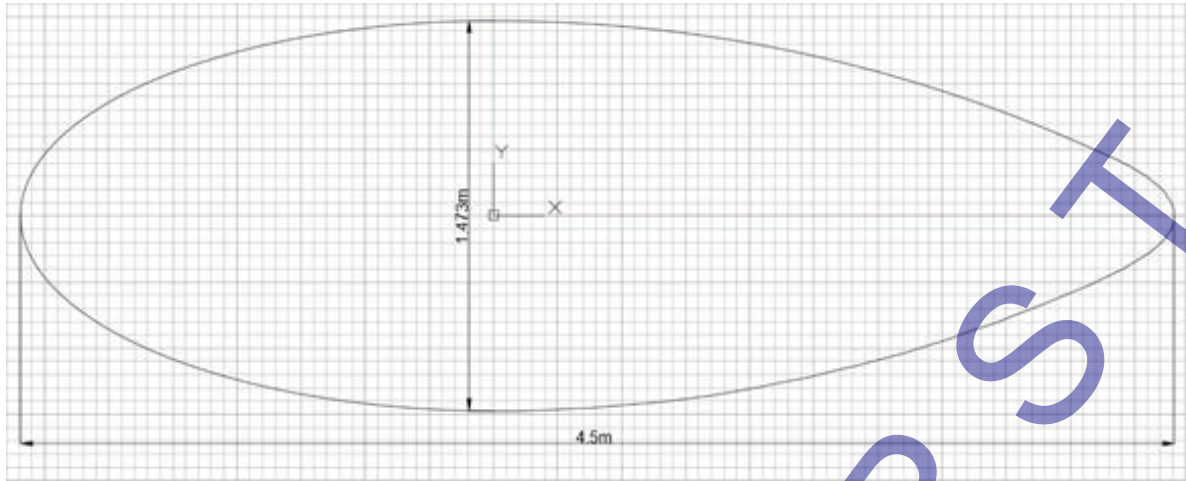

Fig. 6. 2D Model for L=4.5m GNVR shape

3.2 Sizing of Airship

Following the GNVR shape nomenclature, the length of the airship is assumed to be 4.5 m as shown in Figure 6. The remaining parameters were calculated once the maximum diameter of the envelope was determined and are presented in Table 4.

Table 4. Measured parameters

Parameter	Value
Length	4.5 m
Volume	4.772 m^3
Surface area	16.26 m^2
Net lift	319.88 g
Reynolds Number	0.9187 x 10^6
Cdv_e	0.02733
C_{dv}	0.052135
Envelope drag	1.84455 N
Thrust required	188.1 g
Envelope mass	4113.78 g

The measurements for the airship's tail fin sizing, area ratio, aspect ratio, span-to-chord ratio, taper ratio, and location ratio were obtained from a survey of numerous previous airships and are presented in Table 5. These values are reliable and are currently utilized globally in the development of rudders and stabilizer schematics for many different types of airships. These values yield the aspect ratio, root chord, and tip chord, which are shown in Figure 7 as 0.6585 m, 0.7088 m, and 0.5024 m, respectively.

Table 5. Tail fin estimation ratios

Fin Parameter	Formula	Value
Total area of 4 fins	S_{fin}	0.9658 m^2
Area Ratio	S_{fin}/S_{env}	0.0594
Aspect Ratio	$4b^2/S_{fin}$	0.6585
Span to Chord Ratio	b/C_r	0.5625
Taper Ratio	C_t/C_r	0.7083
Location Ratio	L_{fin}/L_{env}	0.8000
Fin weight	-	350.539 g

Journal of Applied Engineering Science

Vol. 22, No. 4, 2024

www.engineeringscience.rs

iipp

publishing

Sudhir Jain Prathik et al. - Innovative airship design for real-time air quality monitoring using IoT technology
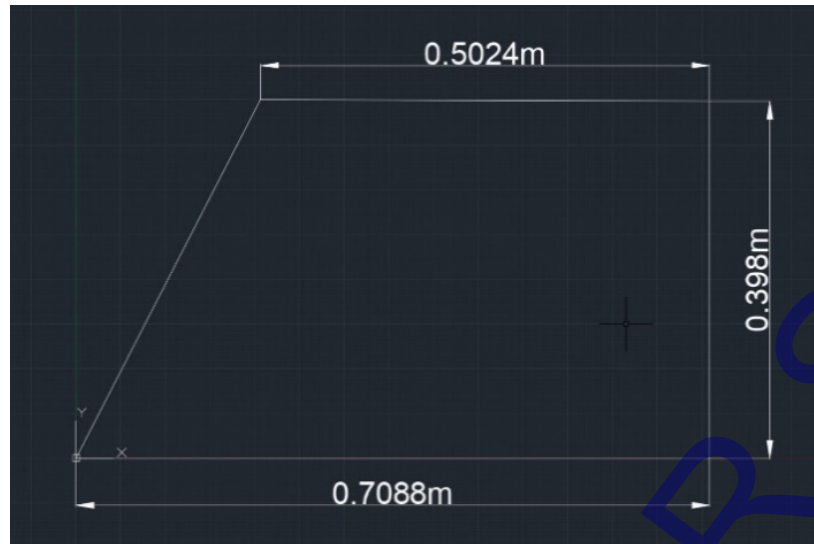
Fig. 7. 2D Model of tail fin

3.3   Endurance

Achieving an endurance of over one hour surpasses the capabilities of most UAVs, making endurance the primary performance parameter. It is a measurement of how long an airship can stay in air before recharging. An airship's endurance is determined by a number of factors such as its size, weight, type, propulsion system efficiency, and fuel capacity. While some airships have shorter endurance because of their size or mission needs, others may be built for long-distance travel and may stay in the air for several days or even weeks at a time.

For the thrust motor selected based on the drag produced by the airship combined with a battery to power the motor with the weight constraint, the endurance can be calculated using Equation (15) at 40.2 mins.

$$\text{Battery Capacity} = \text{No. of motors} * 1000 * \text{Amps consumed} * \text{time (hr)} \quad (15)$$

The endurance that is produced is more efficient than a drone for that particular payload and cost, making it a better option to use an airship instead of a drone for high-endurance missions.

3.4   Stability aspects

For an airship, the center of gravity (C.G) and the center of buoyancy (C.B) are the two main parameters that must be considered to make the airship stable when there is gust or cross winds. The center of gravity of the body is the point at which the total gravitational force of the body can be considered to act. The center of buoyancy is the center of gravity of the volume of water displaced by the body when immersed in water. Determining the center of gravity is important for any flying object. In general, determining the C.G is a complicated procedure because mass (and weight) may not be uniformly distributed throughout the object. From Gawale et al. [17], Xcg is calculated based on the weight breakdown of various components of the aircraft and then the Xcg of the entire airship is calculated to be 2.12 m from the nose. The center of buoyancy for the simple shapes is the centroid of the body. However, for complicated shapes such as airships, there are some errors in their location, and both of them are not the same. Hence, to find the center of buoyancy, the entire airship was divided into known shapes, and using the area average method, the center of buoyancy was found to be 2.103 m from the nose, as shown in Figure 8.

Both the center of gravity and the center of buoyancy of the airship were determined using the above techniques. For the airship to be statically stable, its C.G. should be below the C.B. of the airship. To achieve this, the gondola was placed 2.04 m from the nose. If the positions are reversed, the airship is unstable and tilts upside down during the mission operation.
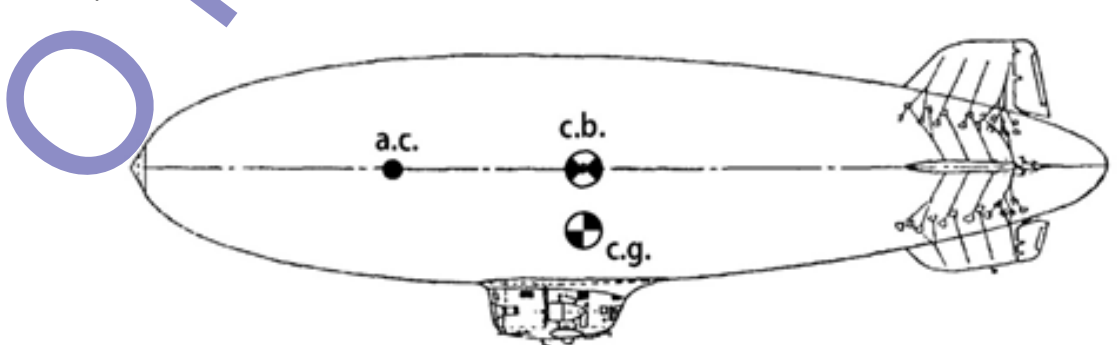

Fig. 8. Stability criteria for airship

3.5 Fabrication process

The 2D drawing of the petal was created using the measured geometric data, with x being the airship's overall length of 4.5 meters. To create a smooth curve, the coordinates of the petals are connected, and the complete petal is broken up into several A4-sized sheet drawings that can be printed. It is necessary to use moderate pressure and temperature to seal the petals between the two layers. This procedure was conducted in Hitech Pack, Bengaluru, Karnataka, India.

The gondola is made of Depron and has dimensions of 40 mm × 10 mm × 8 mm to ensure that the payload fits inside. To ensure that the free-stream air makes direct contact with the sensors and provides precise information, two holes are drilled in the front for the sensors to be attached. To accommodate the motors, a 60 mm carbon fiber rod is positioned in the middle of the gondola. This rod generates sufficient yaw moment to enable the airship to make necessary turns. The necessary support at the junction of the gondola and rod is provided by two 3D printed mounts, which are further strengthened from the inside using balsa wood. The complete fabrication process is illustrated in Figure 9.
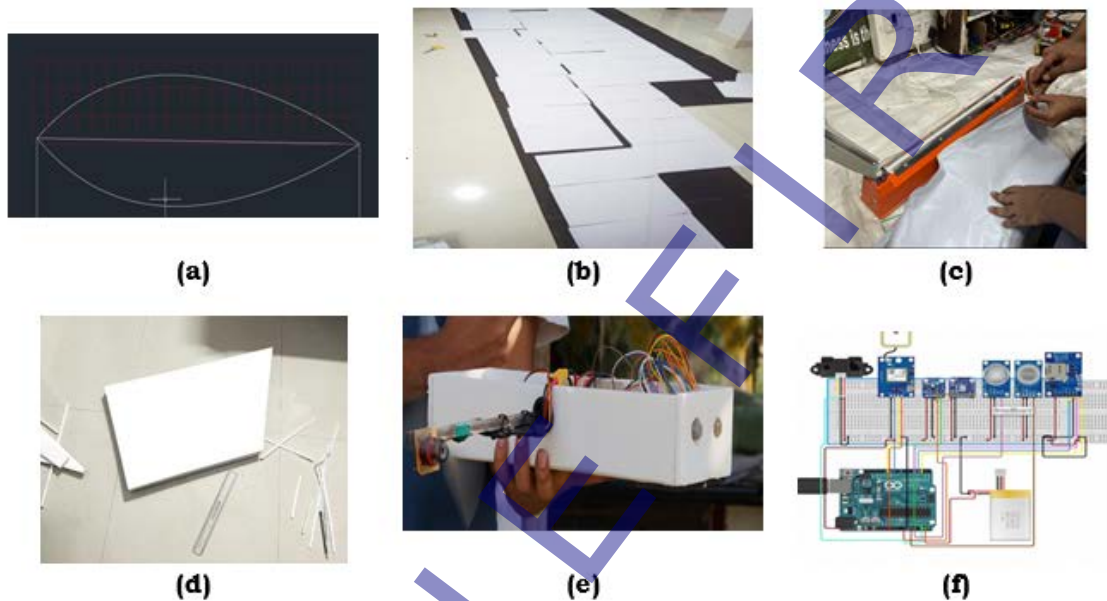

Fig. 9. Fabrication Process (a) 2D Drawing of GNVR Petal, (b) Petal Cutting Process, (c) Heat Sealing Process, (d) Tail Fin Fabrication, (e) Gondola Setup and (f) Circuit Connection of Sensors

3.6 Testing and results

Technical failures, environmental concerns, and regulatory issues are among potential risks associated with airships. Among those factors, the Helium leak test was chosen in our current investigation as the probable concern. The airship was initially filled with ambient air, and then repeatedly tested before being filled with helium. This was done to check for leaks and determine how the material of the envelope responds to the pressure from the gas inside. Areas involving overlapping petals, such as the nose, tail, and nozzles, were found to have minor leaks, which were patched with tape, glue, and adhesive material. Finally, the airship was filled with 5 m^3 of helium and tested, as illustrated in Figure 10.

Fig. 10. Airship filled with helium

Journal of Applied Engineering Science

Vol. 22, No. 4, 2024
www.engineeringscience.rs

iipp
publishing

Sudhir Jain Prathik et al. - Innovative airship design for real-time air quality monitoring using IoT technology

After the gondola was attached, the propellers were turned on. The airship gradually began to fly and reached the required altitude owing to the dynamic lift produced by the airship. To evaluate stability, a variety of maneuvers were executed, including rolling and turning. Tables 6 and 7 summarize the tests and outcomes. During this period, the live sensor measured pollution data are visualized and analyzed using ThinkSpeak IoT cloud platform using a laptop, and it was ensured that the data were continually fed.

Table 6. Flight test results

Type of Test	Observation	Action Taken
Helium leak test 1 (visual)	A large hole (20 mm size) at the intersection of petals	Patched the hole with envelope material using strong adhesive.
Helium leak test 2 (visual)	Leak from nose of airship (3-4 mm size)	Bonded the intersection of petals using adhesives
Helium leak test 3	No visible flaws in the airship, but there is a steady leak through the fabric itself, resulting in a volume reduction of around 10% of helium.	Noted to keep the pressure at 1 bar to reduce leakage through the envelope. (Use of Teflon spray dramatically minimizes the leaks.)
Flight test- 1	Airship is found tail heavy and requires ballast at nose or reduction of tail weight.	Since the airship is fairly stable, three fins are employed instead of four to minimize tail weight, and the gondola is repositioned closer to the nose.
Flight test-2	The airship is stable in roll and yaw, yet control felt difficult.	Active controls are intended to be located in the tail rather than the gondola

Table 7. Average sensor results

Particulars	Value
CO	0.621 ppm
CO_2	0.350 ppm
SO_2	0.004 ppm
C_6H_6	0 ppm
Pressure	912 MPa
Altimeter	878 m
Temperature	302.67 K

By incorporating the design features like modular payload bays, flexible mountings, providing dynamic control of altitude and speed, weather resistant upgrades and advanced communication systems the airship can be easily customized to meet a wide range of mission requirements and accommodate additional sensors, making it a versatile tool for environmental monitoring, research, and other applications.

4 CONCLUSIONS

Employing an airship is a viable method for accurately monitoring air quality data. Because the sensors directly measure the air quality data, the obtained data are more reliable than existing methods, such as ground stations, which require interpolation of values to arrive at the required value. Moreover, it is a cost-effective method for measuring air pollutants. Although it is less expensive, the scarcity of helium makes it expensive; hence, research has to be conducted to use hydrogen as an alternative in a safer manner. This will significantly lower the cost, even further. An airship can gather data and survey broad areas because it is moveable and remotely operated. Real-time data transfer without range limitations is made possible by modern technologies, such as the Internet of Things. A major challenge in the fabrication process is the heat sealing of the petals to create an envelope shape. After heat-sealing, it was difficult to obtain the correct shape. As a result, strong adhesive tapes are required, which may slip off the envelope's surface owing to heat absorption from sunlight.

5 ACKNOWLEDGMENT

6 REFERENCES

[1] Tillmann, R., Gkatzelis, G.I., Rohrer, F., Winter, B., Wesolek, C., Schuldt, T., Lange, A.C., Franke, P., Friese, E., Decker, M., Wegener, R. (2022). Air quality observations onboard commercial and targeted Zeppelin flights in Germany–a platform for high-resolution trace-gas and aerosol measurements within the planetary boundary layer. Atmospheric Measurement Techniques, vol. 15, no.12, 3827-3842, DOI: 10.5194/amt-15-3827-2022

[2] Manikandan, M., Pant, R. S. (2021). Research and advancements in hybrid airships-A review. Progress in Aerospace Sciences, vol. 127, 100741, DOI: 10.1016/j.paerosci.2021.100741

[3] Liao, L., Pasternak, I. (2009). A review of airship structural research and development. Progress in Aerospace Sciences, vol. 45, no.4-5, 83-96, DOI: 10.1016/j.paerosci.2009.03.001

[4] Dorrington, G. E. (2006). Drag of spheroid-cone shaped airship. Journal of aircraft, vol. 43, no.2, 363-371, DOI: 10.2514/1.14796

[5] Gangadhar, A., Manikandan, M., Rajaram, D., Mavris, D. (2021). Conceptual design and feasibility study of winged hybrid airship. Aerospace, vol. 9, no.1, 8, DOI:10.3390/aerospace9010008

[6] Mang. C., Yiping, L. (2017). Flat type airship. Patent for the invention CN 205931210 U, 08.02.2017. Application no. 201620742910 dated 14.07.2016.

[7] Bock, J. K., Künkler, H. (2015). Concept of a Lenticular Hybrid Airship Using Hydrogen for Multiple Operation Modes. 10th International Airship Convention 2015, p 1-6.

[8] Fazakas, Gabor. (2000). Hybrid Toroidal Airship. Patent published for the invention WO 2000032469 A1, 08.06.2000.

[9] Suefuku, H., Hirayama, T., Hirakawa, Y., Takayama, T. (2010). Torus-type airship aiming at high airworthiness quality. 27th international congress of the aeronautical sciences 2010, p. 1-10.

[10] Powell, J., Folsom, C.A. (2011). High altitude two balloon airship. Patent for the invention US 8061647 B1, 22.11.2011. Application no. 12/082420 dated 10.04.2008.

[11] Manikandan, M., Shah, R. R., Priyan, P., Singh, B., Pant, R. S. (2024). A parametric design approach for multi-lobed hybrid airships. The Aeronautical Journal, vol. 128,1-36, DOI: 10.1017/aer.2023.37

[12] Pope, C. (2004) "The big lift," Professional Engineering, vol. 17, no. 8, 24-25.

[13] Sighard Hoerner, F. (1965). Fluid-dynamic Drag. Hoerner Fluid Dynamics, Bakersfield, CA 93390

[14] Pant, R. S. (2008). Methodology for determination of baseline specifications of a nonrigid airship. Journal of Aircraft, vol. 45, no.6, 2177-2182. DOI: 10.2514/1.34858

[15] Sonawane, B. S., Fernandes, M. A., Pant, V., Tandale, M. S., Pant, R. S. (2014). Material characterization of envelope fabrics for lighter-than-air systems. International Colloquium on Materials, Manufacturing and Metrology 2014.

[16] Shaikh, A., Inamdar, J. A., Saleem., Sayyed Mufeed Fidae. (2015). Design and development of indoor airship; gondola (fixed and sliding), avionics, nose batten. Thesis, School of Engineering and Technology, Anjuman-I-Islam's Kalsekar Technical Campus, New Panvel.

[17] Gawale, A.C., Raina, A.A., Pant, R.S., Jahagirdar, Y.P. (2008). Design, Fabrication and Operation of Remotely Controlled Airhips in India. 26th international congress of the aeronautical sciences 2008, p. 1-12.